ISBN: 978-628-96613-3-0. ISSN: 2414-6390. Digital Object Identifier: https://dx.doi.org/10.18687/LACCEI2026.1.1.1280

Design of a Modular Mobile Robot with Active Suction for Glass Window Cleaning in Buildings

Joaquín Fabio Gonzales Rodríguez[1], Henry Edgardo Torres Quiñones[2], Marcelo Jaime Quispe Ccachuco[3], César Pío Castillo Cáceres[4], Christiam Guillermo Collado Oporto[5], Alfredo Andrés Guzmán Valdivia[6]
[1,2,3,4,5,6] *Universidad Católica de Santa María, Perú, joaquin.gonzales.rodriguez.2003@gmail.com, henry.ed.52@gmail.com, mquispec@ucsm.edu.pe, ccastill@ucsm.edu.pe, ccollado@ucsm.edu.pe, aguzman@ucsm.edu.pe*

Abstract*– Window cleaning in high-rise buildings is a high-risk activity that demands automated solutions to ensure industrial safety and operational efficiency. This paper presents the design, prototyping, and validation of a modular mobile robot with active suction, optimized for glass facade maintenance. The system utilizes high power brushless motors to generate controlled suction, paired with a differential locomotion system for stable vertical displacement. A technical contribution is the design of reconfigurable architecture, allowing the integration of interchangeable modules for cleaning, structural inspection, or monitoring. The firmware, developed using Object-Oriented Programming (OOP), enables robust logical management of peripherals and sensors, facilitating seamless system configuration. To validate the approach, a functional prototype was evaluated under real conditions, focusing on load capacity, aerodynamic stability, and adhesion reliability. Results demonstrate constant suction and effective trajectory control, significantly reducing human risk in critical environments. Furthermore, this research establishes the basis for future autonomous navigation and sensor integration in large-scale urban settings. Consequently, this mechatronic development represents a substantial advancement in automating specialized services for smart city infrastructure. By providing a versatile and safe platform, this work addresses the inherent challenges of high-altitude maintenance while establishing a scalable framework for diverse vertical robotic applications in modern construction.

***Keywords*-- Robot, Modularity, Suction, Cleaning, OOP.**

I. INTRODUCTION

The maintenance and cleaning of vertical surfaces in high-rise buildings represent a complex and high-risk task for human operators, primarily due to extreme working conditions at height and exposure to adverse environmental factors. As D. Schmidt and K. Berns discuss in their survey of design aspects, mobile robotics applied to vertical structures has emerged as a transformative technological alternative capable of enhancing safety, efficiency, and repeatability in these operations [1].

Climbing robots, commonly referred to as wall-climbing robots, are generally classified by their adhesion mechanisms. In this regard, G. Fang and J. Cheng emphasize that active suction has proven to be one of the most effective methods for smooth surfaces like glass due to its versatility and relative simplicity of implementation [2].

To ensure a reliable grip, the suction force must overcome both gravity and external disturbances. This requires a precise balance between the pressure differential and the volumetric flow needed to compensate for air leakage at the chassis-surface interface (see Fig.1).

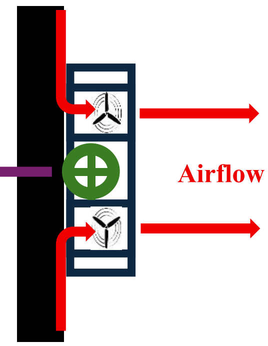

Fig. 1 Representation of Adhesion Forces and Airflow Dynamics

The leakage flow rate can be modeled by considering the discharge coefficient and the effective area of leakage, which, as demonstrated by T. T. Tun et al., are critical for maintaining the necessary negative pressure through suction systems [3].

$$Q = C_d * A_{\text{leak}} * \sqrt{\frac{2*\Delta P}{\rho}} \quad (1)$$

Furthermore, the operational performance of the suction system is directly linked to the angular velocity of the impellers. Achieving the target pressure differential requires estimating the turbine speed required to move the calculated airflow.

$$\sqrt{\frac{2*\Delta P}{\rho}} = \pi * D * n \quad (2)$$

Ultimately, the mechanical power required to sustain this vacuum state is defined by the product of the differential pressure and the flow rate. Understanding these fluid dynamics is essential for sizing the high-power brushless motors used in this prototype.

$$P_{\text{mec}} = \Delta P * Q \quad (3)$$

However, as L. Wijayathunga et al. pointed out, autonomous navigation in these unstructured outdoor environments continues to face significant technical hurdles regarding real-time scene understanding and movement stability [4]. This necessitates robust teleoperation systems that allow for human-in-the-loop control. A critical strength of this work, aligned with the integrated control strategies proposed by Y.-S. Lee et al., is the implementation of a high-speed wireless communication link that minimizes latency, ensuring that operator commands are translated into physical motion with minimal delay even at significant distances [5].

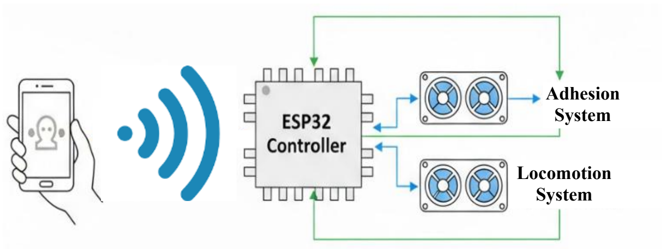

Fig. 2 Teleoperation Control Loop

Current literature reports diverse approaches to optimizing window cleaning. For instance, M. A. V. J. Muthugala et al. introduced the concept of "adhesion-awareness" to dynamically adjust suction force based on internal system pressure [6]. While some designs, such as the one by K. Rambhad et al., have prioritized mechanical simplicity to ensure ease of manual operation, more advanced systems [7], like those developed by R. S. Bisht et al., have integrated trajectory optimization and dynamic control to maximize cleaning efficiency on glass facades [8]. Despite these breakthroughs, many existing robots suffer from limited autonomy due to tethered power sources or excessive weight, a challenge also noted by Lee et al. [5]. Recent research by A. Abhijith Kumar et al. has validated, through simulations, the use of vacuum cups and semi-automatic cleaning modules [9], while J. Liu et al. focused on the optimization of adsorption systems and adhesive belts to improve traction and payload capacity. [10].

A critical factor identified in the current state of the art is the lack of operational flexibility. As A. Brunete et al. argue, most devices are purpose-built for specific functions, which limit their adaptability to diverse architectural scenarios [11]. This gap motivates the transition toward modular reconfigurable robotics, a field where J. Seo et al. has shown that modularity allows robots to be self-configurable, adapting their structure to the required task [12]. According to L. A. T. Vu et al., trends in this field focus on reconfigurable designs that allow for multi-plane transitions [13]. Recent developments by B. Wang et al. further explore modular cleaning capabilities [14], while Q. Zhang et al. have proposed hybrid adhesion designs to manage complex internal transitions [15]. To handle this inherent complexity, D. J. Miller and R. C. Lennox suggest that an integrated control system is required to manage the robot's subsystems effectively. [16].

Software architecture is equally vital for modularity. C. Zieliński maintains that the Object-Oriented Programming (OOP) paradigm serves as an essential methodology for modern robotic software development [17], allowing for the creation of robust and scalable environments as described by S. Maclean and S. Smith [18]. Implementing OOP in firmware, as C. Gu explains, facilitates the logical management of peripherals and sensors using languages such as C++, optimizing the system architecture from the initial coding phase [19]. Finally, the rigorous application of standardized frameworks, such as the VDI 2206 V-model discussed by I. Graessler and J. Hentze, ensures a seamless interdisciplinary integration of mechanical, electronic, and software domains. [20].

This work presents the design, prototyping, and validation of a modular mobile robot with active suction, specifically optimized for building window cleaning. By combining a robust mechanical adhesion system with an OOP-based software architecture, this project provides a scalable platform that reduces human risk while increasing maintenance efficiency in modern urban infrastructures.

II. Materials and Methods

The development of the modular climbing robot is governed by the VDI 2206 German standard, which provides a structured framework for the design of mechatronic systems. This methodology utilizes the "V-Model," ensuring a seamless integration of mechanical engineering, electronics, and control software through iterative cycles of requirements engineering, system design, and cross-domain validation.

A. *Requirements and System Abstraction*

The initial phase focuses on defining the operational environment and constraints. The primary problem addressed is the high-risk nature of cleaning glass facades in high-rise buildings, which requires a system that is lightweight, highly adhesive, and capable of autonomous or assisted navigation.

To define the system's interaction with its environment without considering internal complexities, a Blackbox Diagram was developed (see Fig. 3). In this model, the system is viewed as a functional unit that transforms inputs into desired outputs. The main inputs consist of electrical energy and wireless control signals. The outputs include the resulting cleaning force, kinetic displacement across the vertical plane, and real-time operational status data reported to the user interface.

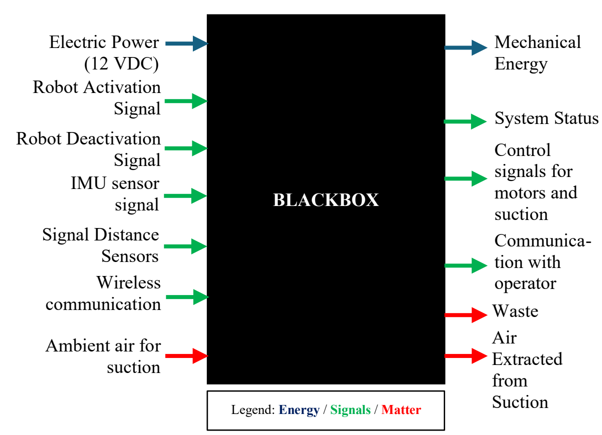

Fig. 3 System Blackbox Diagram

B. *Functional and Operational Decomposition*

Following the requirements definition, the main function of Window Cleaning Optimization was decomposed into sub-functions. This functional hierarchy ensures that each mechatronic subsystem contributes directly to the project's success. The system comprises three critical components: an active suction system for adhesion management to ensure vertical stability, a differential drive mechanism for locomotion and kinematics, and proximity sensors for sensing and collision avoidance to navigate obstacles and edges safely on high-altitude facades.

This decomposition allows modular architecture, where the cleaning head or sensing modules can be swapped without altering the core locomotion or adhesion control logic (see Fig. 4).

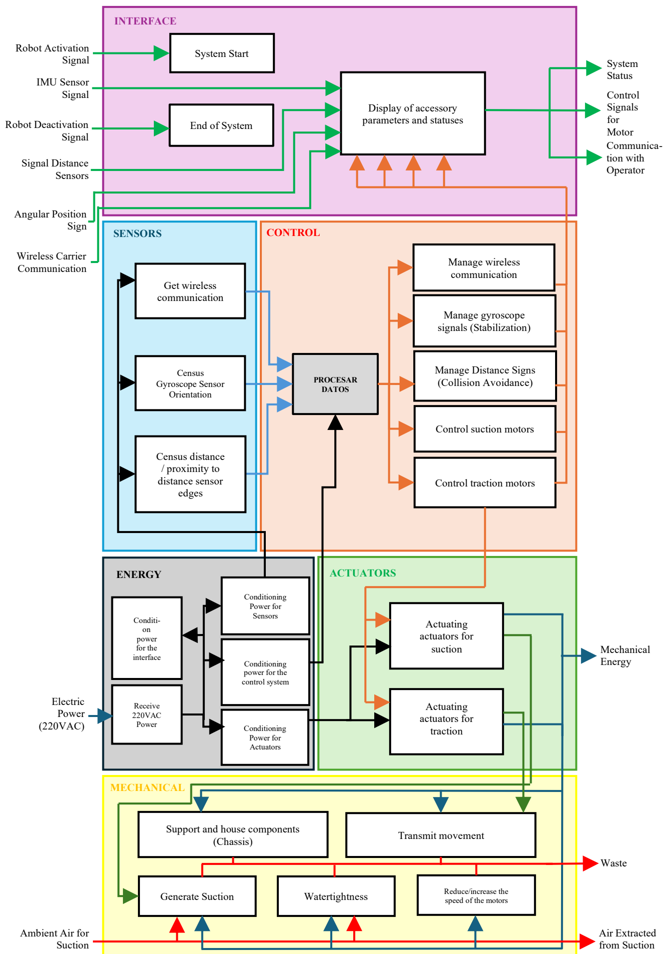

Fig. 4 Robot Functional Structure.

C. *Evaluation and Selection of the Optimal Alternative*

To identify the best design configuration, a Morphological Matrix was utilized to explore technical solutions for each sub-function. The resulting design candidates were subjected to a rigorous Technical-Economic Analysis to evaluate criteria such as adhesion safety, ease of handling, and manufacturing costs.

In the first stage, a technical evaluation was conducted, where three design solutions were assessed using a weighted scoring method, from 0 to 5. Higher weights were assigned to critical factors such as energy efficiency, stability, and modularity based on their impact on system performance.

TABLE I
TECHNICAL EVALUATION MATRIX

Technical Analysis						
S: Score from 0 to 5						
0=Not satisfied, 1=Acceptable, 2=Sufficient, 3=Ok, 4=Very well, 5=Ideal						
G: Gains						
Solutions			Solution 1	Solution 2	Solution 3	Ideal
N°	Evaluation Criteria	G	S	S	S	S
1	Good use of energy	4	5	4	3	5
2	Security	5	5	5	3	5
3	Speed	5	5	4	3	5
4	Stability	5	5	5	3	5
5	Rigidity	4	5	4	3	5
6	Handling	4	3	4	5	5
7	Ease of operation	4	3	5	4	5
8	Transportability	4	3	4	5	5
9	Quality of Work	5	5	5	3	5
10	Complexity	3	2	4	5	5
Maximum Score			182	188	151	215
Technical Value			0.847	0.874	0.702	1.000

Simultaneously, an economic feasibility study was conducted to normalize implementation costs against a baseline budget, considering assembly time and component count.

TABLE II
ECONOMIC EVALUATION MATRIX

Economic Analysis						
S: Score from 0 to 5						
0=Not satisfied, 1=Acceptable, 2=Sufficient, 3=Ok, 4=Very well, 5=Ideal						
G: Gains						
Solutions			Solution 1	Solution 2	Solution 3	Ideal
N°	Evaluation Criteria	G	S	S	S	S
1	Number of Pieces	4	2	4	5	5
2	Ease of Assembly	4	3	5	5	5
3	Productivity	5	4	5	3	5
4	Miscellaneous Costs	5	2	4	4	5
5	Minimal waste	3	3	4	5	5
Maximum Score			55	93	92	105
Technical Value			0.524	0.886	0.876	1.000

The selection was finalized by plotting the Technical (X) and Economic (Y) values on a comparative graph (see Fig. 5). Solution 2 emerged as the optimal choice, demonstrating the best balance between high-performance vertical adhesion and cost-effective modular implementation. This solution was selected for the detailed engineering and prototyping phases, as it aligns most closely with the "Ideal Point" of efficiency and financial viability.

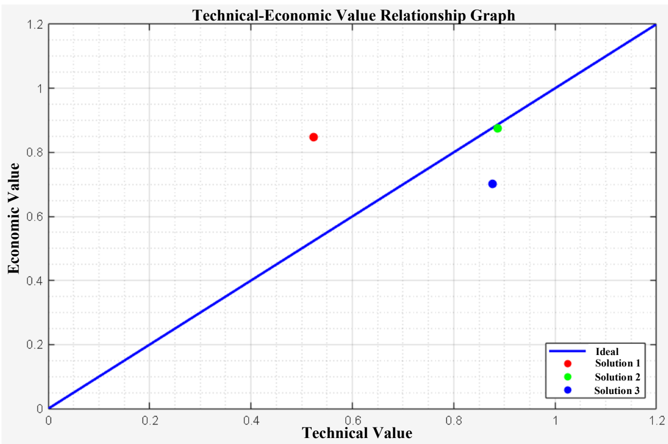

Fig. 5 Technical-Economic Value Relationship Graph.

D. Mechanical Design

1) Suction System Sizing

The adhesion system utilizes a circular vacuum chamber with a diameter D = 0.133 m, resulting in an effective suction area of 0.013892 m^2. Given a robot mass of 2.5 kg and applying a safety factor of 2, the system was dimensioned for an equivalent mass of 5 kg. The minimum force required to counteract gravity is:

$$F = m * g \quad (4)$$

Where g = 9.81 m/s^2. Assuming that the load is distributed between two support points, an effective force of 2.5 kg per point was considered.

Regarding the traction behavior on vertical glass surfaces, the coefficient of friction between the robot tracks (rubber-based material) and the glass was assumed to be constant, based on technical literature values for rubber–glass contact under dry conditions. Consequently, no explicit calculation of traction coefficient variation or torque margin was performed in this stage. The design approach prioritized ensuring sufficient adhesion force through the suction system, as maintaining normal force is the dominant factor in guaranteeing traction capability. The minimum differential pressure required is calculated as:

$$F = \Delta P * A \quad (5)$$

Based on this, a ΔP of 1.77 kPa was calculated. This is the minimum differential pressure the chamber must maintain for the suction to support the weight. To size the brushless motor for the turbine, it is necessary to determine the airflow required to maintain that ΔP, accounting for air leaks and imperfect sealing. The dimensions used for this calculation are shown in the following figure:

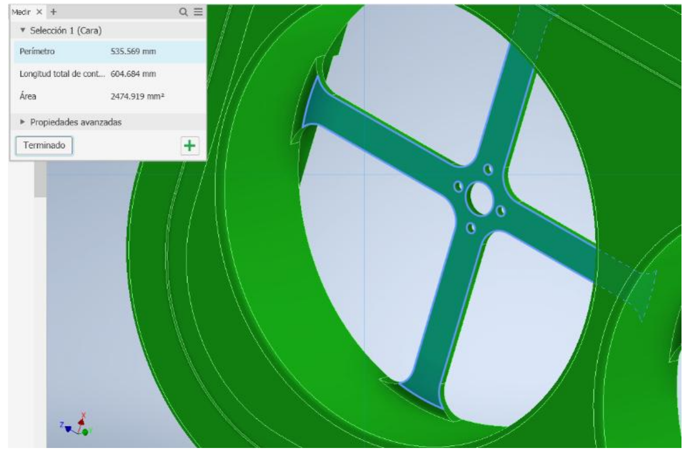

Fig. 6 Measurement of Airflow Obstructions.

The effective area of leakage A_{leak} was determined by subtracting the area of internal structural obstructions (shown in Fig. 6) from the total chamber area, resulting in A_{leak} = 0.0114 m^2. The leakage flow rate is determined by:

$$Q = C_d * A_{\text{leak}} * \sqrt{\frac{2*\Delta P}{\rho}} \quad (1)$$

Where ρ = 1.2 kg/m^3 is the air density and the discharge coefficient C_d is set at 0.6, a standard value for experimental leakage in non-hermetic seals. Based on these values, an approximate flow rate of Q = 0.372 m^3/s was obtained.

The required angular velocity of the turbine was estimated as follows:

$$\sqrt{\frac{2*\Delta P}{\rho}} = \pi * D * n \quad (2)$$

This calculation yields an approximate speed of 10000 RPM. The minimum mechanical power required to maintain the vacuum was then calculated as:

$$P_{\text{mec}} = \Delta P * Q \quad (3)$$

This results in a value of approximately 656.7 W. Considering an overall efficiency of 85 %, the required electrical power was estimated as:

$$P_{\text{elec}} = \frac{P_{\text{mec}}}{\eta} \quad (6)$$

Leading to a final value of approximately 773 W.

To meet this demand, 2300 kV brushless motors were selected. While these motors can reach a peak consumption of 60 A (approx. 720 W at 12 V), this value represents an absolute maximum. In practice, the operating current is estimated at 30 A or less, as peak amperage is rarely sustained during stable adhesion.

2) Structural Analysis of the Vacuum Chamber

The vacuum chamber was designed using ABS to prioritize system lightness and analyzed by applying a uniform pressure equivalent to the previously calculated differential pressure of 1.77 kPa, distributed over the internal surfaces of the chamber (see Fig. 7). The simulation was performed using a parabolic tetrahedral mesh with an average element size of 2.0 mm to ensure convergence.

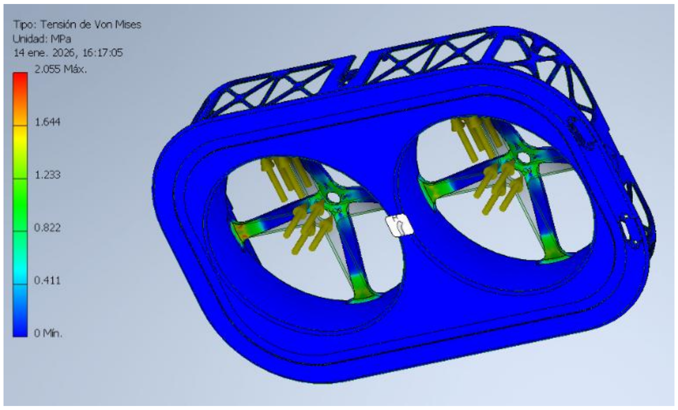

Fig. 7 Von Mises Stress Results – Chassis Analysis.

On the other hand, the fixed constraint was established across the entire bottom area. The structural analysis yielded a maximum Von Mises stress of 2.055 MPa (see Fig. 7), a value significantly lower than the material's yield strength.

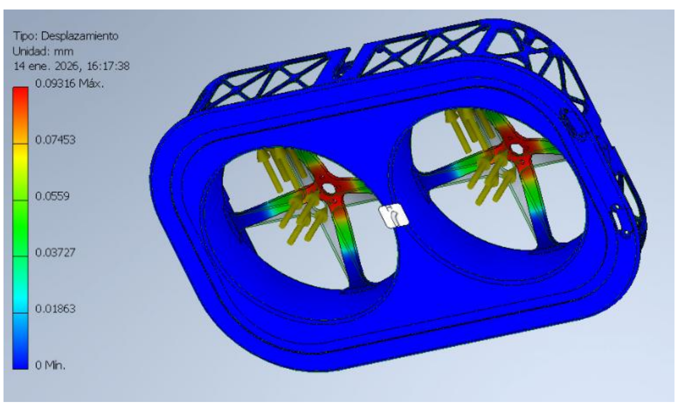

Fig. 8 Displacement Results – Chassis Analysis.

The maximum recorded displacement was 0.093 mm (see Fig. 8), which is considered negligible for the system's operation. These results confirm that the mechanical design possesses adequate structural safety margins and is suitable to operate as the base platform for a modular climbing mobile robot. For long-term operations, structural reinforcements or composite materials are proposed to mitigate potential plastic creeps under sustained negative pressure.

3) Design of the Cleaning Module

This section presents the conceptual design and functional framework of the cleaning module, though its physical implementation and experimental validation are beyond the current scope of this study. Developed under a functional approach, the design prioritizes autonomy in particle removal. As illustrated in the schematic (see Fig. 9), the module proposes a compact architecture with an internal micro-pump to manage water supply through a conduction channel. This theoretical process is intended to be enhanced by high-absorption cloths and brushes strategically arranged to maximize surface contact. Finally, the assembly is designed to attach to the main platform through a reinforced interface, maintaining the system's modular character. Future research will focus on the prototyping and empirical testing of this module to evaluate water supply flow and cleaning effectiveness.

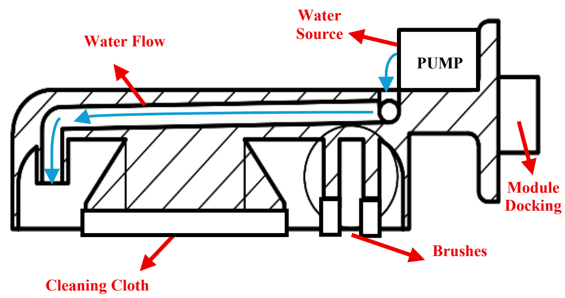

Fig. 9 Cleaning Module Schematic.

4) Integrated System Assembly

The final integration of locomotion, adhesion, and cleaning subsystems results in a cohesive mechatronic platform. As shown in the Exploded View (see Fig. 10), the design features a dual-fan suction system and a differential drive housed within a lightweight chassis. This layout ensures precise alignment between the ESP32 controller and interchangeable modules, maintaining structural integrity at all connection points. The assembly facilitates efficient signal routing and power distribution, demonstrating how the modular cleaning head interfaces with the primary climber for high-altitude tasks.

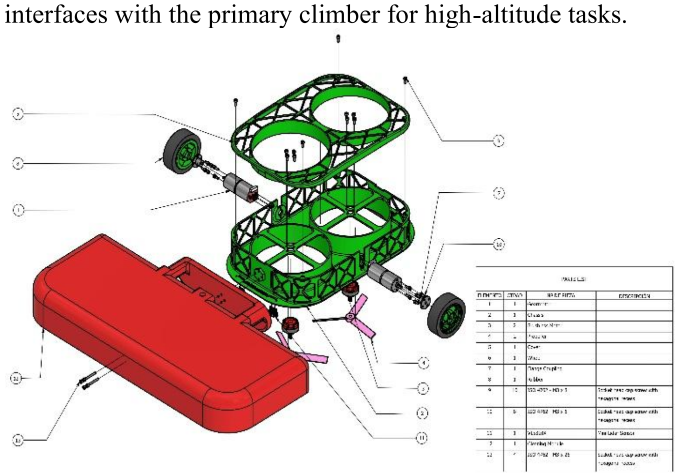

Fig. 10 Exploded View of the Modular Climbing Robot.

E. Electronic Architecture

The system is structured into modular subsystems (power supply, control, locomotion, suction, and cleaning) that are centrally managed by an ESP32 microcontroller. The primary objective of this design is to effectively segregate the high-power stages from the low-power logic circuitry, thereby minimizing electrical noise and ensuring system stability and robust performance.

No dedicated EMI filtering was used for brushless motors. System stability was verified under controlled conditions, though future shielding is recommended to prevent noise-induced transients.

1) Alimentation Architecture and Power Distribution

To handle the robot's heterogeneous power demands, a segregated power-supply architecture was implemented using two main AC/DC sources. A high-capacity 12 V–30 A supply feeds the high-consumption subsystems, including the suction system (two brushless motors driven by ESCs), the locomotion system (two DC motors via an H-bridge), and the water pump (through a relay). A secondary 5 V–3 A supply powers the cleaning subsystem and all low-voltage control electronics, including the ESP32 microcontroller, H-bridge logic circuits, sensor modules (MPU6050 and VL53L0X), optical encoders, and the control circuitry of the ESCs and relay module. As a fundamental design principle, all ground terminals (GND) of both supplies and the ESP32 were interconnected to establish a common 0 V reference, ensuring reliable interfacing between the ESP32's 3.3 V logic signals and modules powered at 5 V and 12 V.

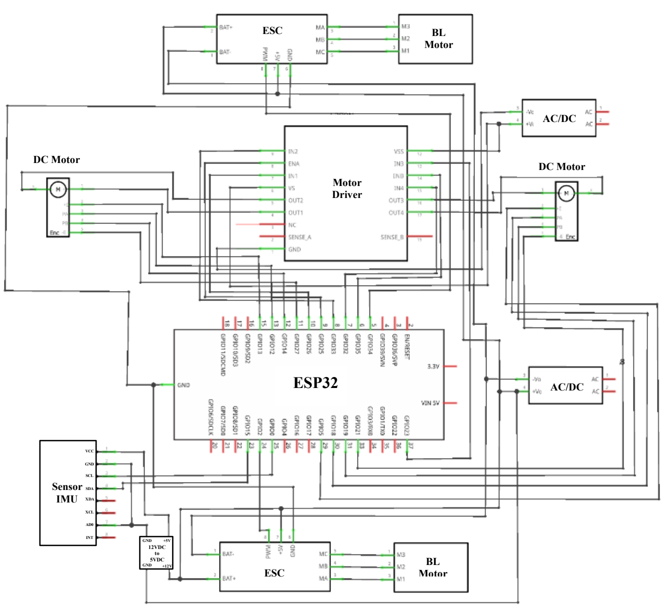

Fig. 11 Electronic Design of the Project.

The robot integrates power supply, control, locomotion, suction, and sensing subsystems; all interconnected through a common ground (GND) reference (see Fig. 11). This unified grounding scheme enables the low-voltage logic signals generated by the ESP32 to reliably control actuators powered at 5 V and 12 V, ensuring stable operation and proper signal integrity across the entire electronic architecture.

2) Central Control System

ESP32 was selected as the central processing unit due to its dual-core architecture, high processing capability, and, fundamentally, its integrated Wi-Fi connectivity, which constitutes the foundation of the teleoperation system.

TABLE III
ESP32 PINOUT

Pin (GPIO)	Function	Sistema	Purpose
GPIO 21	SDA	Control / Sensors	I2C Data Bus
GPIO 22	SCL	Control / Sensors	I2C clock bus
GPIO 16	ESC_1_PWM	Suction	Control signal for ESC 1
GPIO 17	ESC_2_PWM	Suction	Control signal for ESC 2
GPIO 13	LOCO_EN_A	Locomotion	(PWM) Speed Motor DC 1
GPIO 14	LOCO_IN_1	Locomotion	Direction Motor DC 1
GPIO 27	LOCO_IN_2	Locomotion	Direction Motor DC 1
GPIO 12	LOCO_EN_B	Locomotion	(PWM) Speed Motor DC 2
GPIO 26	LOCO_IN_3	Locomotion	Direction Motor DC 2
GPIO 25	LOCO_IN_4	Locomotion	Direction Motor DC 2
GPIO 34	ENCODER_1_A	Locomotion	(Input only) Signal A, Encoder 1
GPIO 35	ENCODER_1_B	Locomotion	(Input only) Signal B, Encoder 1
GPIO 32	ENCODER_2_A	Locomotion	Signal A, Encoder 2
GPIO 33	ENCODER_2_B	Locomotion	Signal B, Encoder 2
GPIO 5	CLEAN_EN	Cleaning	Activate Pump
Vin	5V_IN	Feeding	5V input to power the ESP32
GND	GND	All	Common Ground

F. Software Architecture

1) Control Architecture

In this project, an Object-Oriented Programming (OOP) approach was implemented. The software follows a Super-Loop architecture where all tasks run sequentially in a single thread with equal priority. While this facilitates scalability, a future migration to FreeRTOS is planned to decouple motor control from Wi-Fi communication, ensuring real-time deterministic responses.

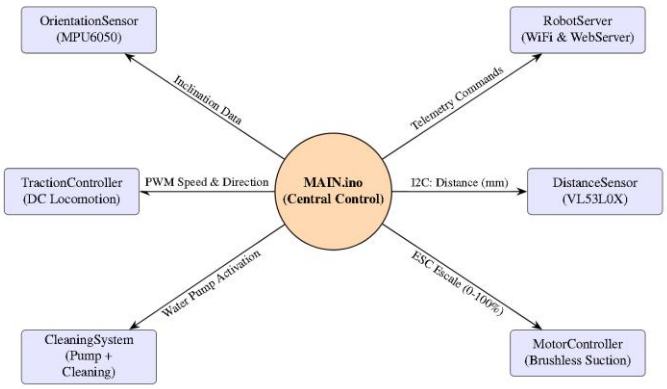

Fig. 12 General Diagram of the Control Architecture.

In the proposed architecture, the main file MAIN.ino acts as the core of the system, coordinating the operation of the different subsystems through instances of specific classes (see Fig. 12). Each class is responsible for managing a particular set of functions within the robot. The RobotServer class handles wireless communication via Wi-Fi and processes commands received from the mobile interface. The MotorController class governs the suction subsystem by controlling the brushless motors through electronic speed controllers (ESCs) to generate adhesion to the glass surface. The DCMotorController class manages the locomotion subsystem by controlling the DC motors and the H-bridge, implementing both tank and differential turning modes to enable robot displacement and maneuverability.

2) Operation of the Main Program

The main program (*MAIN.ino*) enters a continuous loop (see Fig. 13) to handle communication and actuator updates. Currently, the system relies on the ESP32's internal hardware watchdog; however, implementing an explicit software Watchdog is recommended to monitor network latency. Additionally, prioritizing suction and edge detection tasks over the web interface is identified as a necessary improvement to enhance safety during processing peaks.

After initialization of the serial interface, web server, and critical subsystems (vacuum and traction), the program enters a continuous execution loop (see Fig. 13). Within this loop, the system first handles network communication by attending user commands through server.handleClient(). When new data is available, the commanded action, speed, and drive state are extracted. Before executing any motion, a safety check is performed using the VL53L0X distance sensor. If an unsafe distance is detected, the system bypasses the motion logic and directly updates the actuators to prevent collisions.

If the distance is safe, the control logic evaluates the driving mode. When differential mode is disabled, useTankMode is set to true to enable point turns. When enabled, useTankMode is set to false to allow smooth turning. Finally, the functions vacuum.setSpeed() and drive.setMovement() are called to update the suction power and wheel motion, ensuring safe and responsive teleoperation.

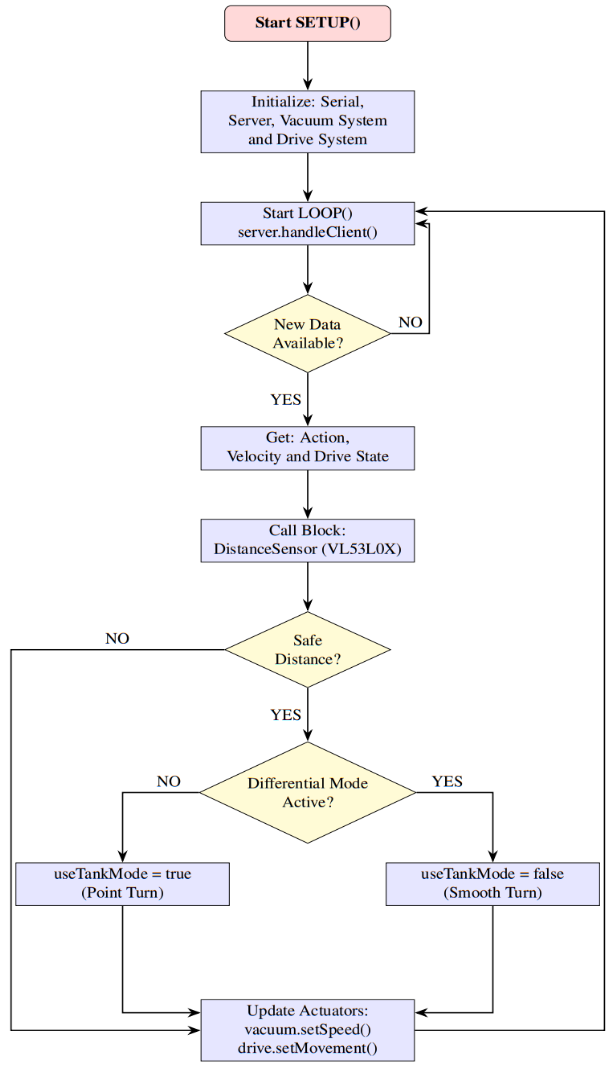

Fig. 13 Flowchart of the loop() function in MAIN.

III. Results and Discussion

A. Prototype Implementation

1) Mechanical Manufacturing and Assembly

The main structure of the robot was manufactured using 3D printing with PLA as the base material, selected for its favorable stiffness-to-weight ratio and rapid prototyping capability. The central chassis, the suction chamber optimized for airflow, and the traction shaft supports were fabricated as separate components.

Subsequently, the locomotion and suction subsystems were assembled. Two DC motors were installed with their corresponding couplings and timing belts to transmit motion to the tracks, ensuring proper tension to prevent slippage. In parallel, two brushless motors were mounted inside the central vacuum chamber, verifying unobstructed impeller rotation. Finally, sealing elements were integrated at the base of the chassis to enhance negative pressure efficiency for vertical adhesion.

The final integration and wiring of the electronic components within the chassis resulted in a compact and organized layout (see Fig. 14).

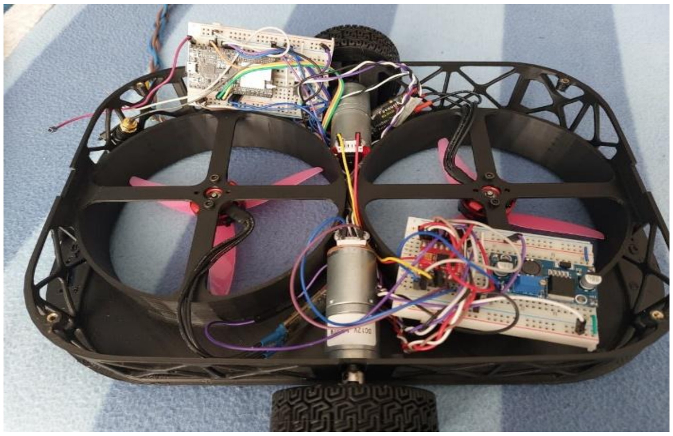

Fig. 14 Integration and Wiring of the Electronic Components within the Chassis.

2) Firmware Deployment and Web Interface

The firmware was deployed by uploading the code developed under the Object-Oriented Programming paradigm to the ESP32 microcontroller. The software, composed of the main file *MAIN.ino* and the modular classes seen in Fig. 10, was successfully compiled, initializing the Wi-Fi communication services and the asynchronous web server.

Once the system was powered on, the robot established a connection to the preconfigured wireless network, enabling access to the teleoperation interface from a mobile device through the assigned IP address. The graphical interface correctly loaded the control elements, including the D-pad, the turning mode selectors (Tank/Differential), and the real-time status indicators (see Fig. 15).

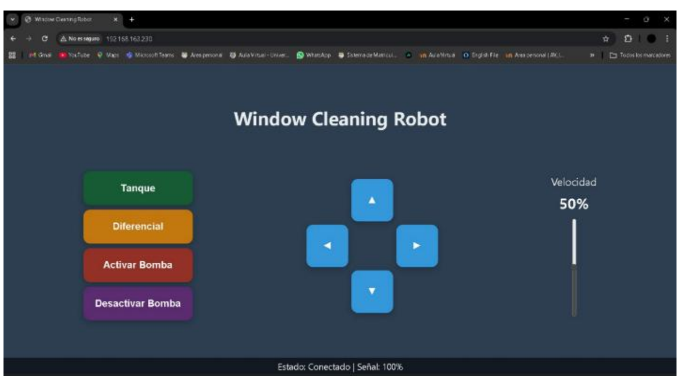

Fig. 15 Web-based control interface deployed and connected through IP address.

B. Functional Tests

1) Connectivity and Teleoperation Tests

Response time was measured via frame-by-frame video analysis at 60 FPS, comparing the web interface interaction with the physical motion of the actuators. This allowed for a direct estimation of latency under real operating conditions, where approximately 85% of the total delay was attributed to the wireless interface (see TABLE IV). The study focused on end-to-end latency; therefore, specific Network Quality of Service (QoS) parameters, such as jitter and packet loss, were not analyzed in this phase and are reserved for future work on communication robustness.

TABLE IV
TELEOPERATION RESULTS AND OPERATIVE SECURITY

Distance (m)	Signal Strength (%)	Total Response Time (ms)	Security Observations
1	100	60	Optimal operation
10	86	277	Fluid response
20	71	518	Perceptible delay
30	55	759	Manual limit control
40	40	1000	Fail-safe limit

The data in TABLE IV reveals a linear trade-off, latency increases as signal strength drops (see Fig. 16). While performance is optimal within 10 meters, the delay reaching a 1000 ms threshold at 40 meters defines a critical safety limit. Although this prototype lacks automatic safety triggers, the results establish that exceeding 30 meters introduces significant operational risk. Consequently, a fail-safe strategy based on these latency thresholds is proposed for future iterations to ensure safe high-altitude teleoperation.

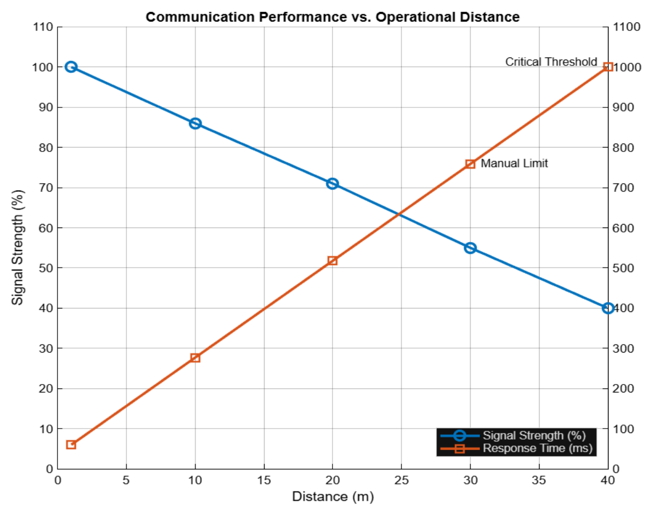

Fig. 16 Correlation between Signal Quality and Control Latency over Distance

3) Suction System Tests

To validate the load-bearing capacity and adhesion performance, static tests were conducted by placing the robot on an indoor vertical glass surface (see Fig. 17). The suction system was activated through the *MotorController* class, gradually increasing the PWM pulse width sent to the ESCs until reaching the nominal operating point calculated during the mechanical design.

The test confirmed that the negative pressure generated by the two brushless impellers, together with the chassis sealing system, produces sufficient adhesion force to support the total weight of the prototype against gravity.

Adhesion performance was verified qualitatively through the ability of the robot to remain attached to the vertical surface under static conditions. No direct measurements of adhesion force, pressure differential (ΔP), or traction were performed due to the absence of dedicated sensors. Therefore, the safety factor was not experimentally quantified but inferred from stable operation. Future work can include calibrated sensors to enable quantitative characterization of the adhesion system.

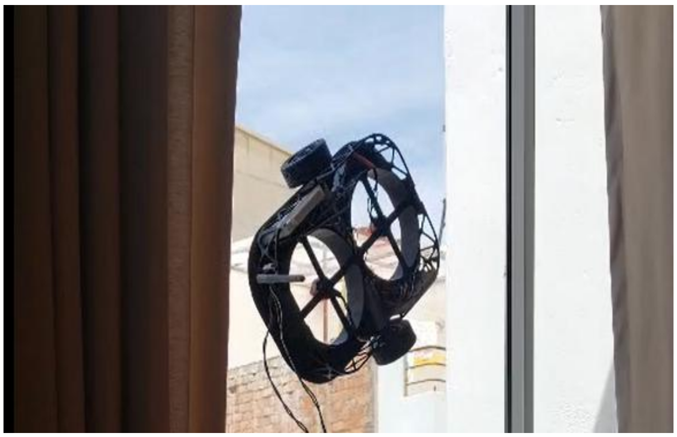

Fig. 17 Static Vertical Adhesion Test Using the Vacuum System.

C. Experimental Validation on a Vertical Surface

Final prototype validation took place in a real-world environment by placing the robot on a vertical glass surface to test the suction and locomotion subsystems simultaneously (see Fig. 18). Initially, the vacuum system was activated at full capacity, confirming that the holding force generated by the brushless motors successfully counteracted gravity. This maintained the robot in a stable static position and validated the initial differential pressure calculations.

Subsequent upward and downward vertical commands were executed while maintaining continuous suction. The results confirmed that the traction motors provided sufficient torque to move the total load, overcoming both track friction and equipment weight. The robot achieved controlled, linear motion across the surface, demonstrating that the control architecture effectively balances the adhesion force required for safety with the mobility needed for cleaning.

Tests were conducted on glass surfaces with a slight layer of dust, which slightly affected adhesion without compromising stability. However, the robot is limited to smooth and flat surfaces. Curved facades may reduce sealing and suction efficiency, while wet surfaces can affect friction and adhesion reliability. These limitations should be addressed in future designs through adaptive sealing mechanisms and enhanced traction control strategies.

Fig. 18 Experimental Validation of the Robot Operating on a Vertical Surface.

D. Scope and Multi-functional Potential

While the experimental results successfully validate the robot's performance in vertical window cleaning, the modular architecture suggests a broader functional potential. The reconfigurable design and stable teleoperation could theoretically support complementary tasks such as structural inspection or environmental monitoring. However, to maintain a well-defined research scope, this study focuses exclusively on cleaning optimization. Modularity was addressed at the design level and was not experimentally validated through physical module exchange. Since the cleaning module was not implemented in the prototype, no functional tests involving module swapping were conducted. Nevertheless, the proposed architecture demonstrates that compatible modules can be designed and integrated through the defined mechanical and electrical interfaces, supporting future expansion of the platform. By concentrating on this primary objective, the research establishes a clear baseline for reliability, which is essential before integrating more complex sensory modules for secondary applications.

IV. CONCLUSIONS

The validation of the prototype against engineering requirements confirms that the mechatronic design and proposed modular architecture are highly effective for high-altitude operations. This work contributes to versatile platforms to the field of cleaning robotics that not only meets functional expectations but also establishes a scalable design standard, allowing future research to focus on task specialization without redesigning the base structure.

A fundamental finding of this research is the optimization of the weight-to-adhesion ratio, resulting in a prototype weighing only 1.7 kg. By designing the suction system to support loads of up to 5 kg, a safety factor exceedingly twice the nominal load was achieved, guaranteeing vertical stability even under environmental disturbances. This surplus capacity represents a critical contribution to industry, as it enables the integration of specialized cleaning heads or heavy sensors without compromising grip integrity on glass surfaces.

From a control perspective, the implementation of Object-Oriented Programming (OOP) in the firmware marks a significant advancement in the logical management of climbing robots. By encapsulating motor and suction control into independent classes, an efficient balance was achieved between high power demand and the protection of control electronics against electrical noise. This modular software approach drastically simplifies the integration of new actuators, facilitating the development of more complex and robust maintenance robots.

Experimental results demonstrated that the differential locomotion system provides the necessary torque to overcome gravity and surface friction, allowing for controlled linear trajectories. Furthermore, teleoperation tests defined an operational safety perimeter of up to 40 meters with fluid response. These findings establish a solid and reliable foundation for the transition toward autonomous navigation in smart city infrastructure maintenance, proving that remote and safe operation is possible in large-scale urban environments.

Finally, the success of the active suction mechanism validates the calculations used to size the high-power brushless impellers. By maintaining sufficient adhesion for vertical stability through an optimized sealing system, the robot achieves a level of adhesion that drastically reduces human exposure to fatal fall risks. This mechatronic development demonstrates that lightweight, modular, and software-optimized platforms are the most viable path toward the full automation of cleaning services for modern building fades.

References

[1] D. Schmidt and K. Berns, "Climbing robots for maintenance and inspections of vertical structures—A survey of design aspects and technologies," *Rob. Auton. Syst.*, vol. 61, no. 12, pp. 1288–1305, Dec. 2013, doi: 10.1016/j.robot.2013.09.002.

[2] G. Fang and J. Cheng, "Advances in Climbing Robots for Vertical Structures in the Past Decade: A Review," *Biomimetics*, vol. 8, no. 1, p. 47, Jan. 2023, doi: 10.3390/biomimetics8010047.

[3] T. T. Tun, M. R. Elara, M. Kalimuthu, and A. Vengadesh, "Glass facade cleaning robot with passive suction cups and self-locking trapezoidal lead screw drive," *Autom. Constr.*, vol. 96, pp. 180–188, Dec. 2018, doi: 10.1016/j.autcon.2018.09.006.

[4] L. Wijayathunga, A. Rassau, and D. Chai, "Challenges and Solutions for Autonomous Ground Robot Scene Understanding and Navigation in Unstructured Outdoor Environments: A Review," *Applied Sciences*, vol. 13, no. 17, p. 9877, Aug. 2023, doi: 10.3390/app13179877.

[5] Y.-S. Lee *et al.*, "The study on the integrated control system for curtain wall building façade cleaning robot," *Autom. Constr.*, vol. 94, pp. 39–46, Oct. 2018, doi: 10.1016/j.autcon.2017.12.030.

[6] M. A. V. J. Muthugala, M. Vega-Heredia, R. E. Mohan, and S. R. Vishaal, "Design and Control of a Wall Cleaning Robot with Adhesion-Awareness," *Symmetry (Basel).*, vol. 12, no. 1, p. 122, Jan. 2020, doi: 10.3390/sym12010122.

[7] K. Rambhad, P. Adhapure, S. B. Lokare, R. B. Navale, and S. E. Zarekar, "Design of Glass Cleaning Robot for High Buildings," *International Journal of Analytical, Experimental and Finite Element Analysis (IJAEFEA)*, vol. 8, no. 1, Mar. 2021, doi: 10.26706/ijaefea.1.8.20210303.

[8] R. S. Bisht, P. M. Pathak, and S. K. Panigrahi, "Design and development of a glass façade cleaning robot," *Mech. Mach. Theory*, vol. 168, p. 104585, Feb. 2022, doi: 10.1016/j.mechmachtheory.2021.104585.

[9] A. Abhijith Kumar, R. K. Akhil, A. A. Ajnas, E. V Abdul Vasih, and J. Jithu, "Modelling and simulation of semi-automatic glass window cleaning machine," *IOP Conf. Ser. Mater. Sci. Eng.*, vol. 1114, no. 1, p. 012057, Mar. 2021, doi: 10.1088/1757-899X/1114/1/012057.

[10] J. Liu *et al.*, "Analysis and optimization of the wall-climbing robot with an adsorption system and adhesive belts," *Int. J. Adv. Robot. Syst.*, vol. 17, no. 3, May 2020, doi: 10.1177/1729881420926409.

[11] A. Brunete, A. Ranganath, S. Segovia, J. P. de Frutos, M. Hernando, and E. Gambao, "Current trends in reconfigurable modular robots design," *Int. J. Adv. Robot. Syst.*, vol. 14, no. 3, p. 172988141771045, May 2017, doi: 10.1177/1729881417710457.

[12] J. Seo, J. Paik, and M. Yim, "Modular Reconfigurable Robotics," *Annu. Rev. Control Robot. Auton. Syst.*, vol. 2, no. 1, pp. 63–88, May 2019, doi: 10.1146/annurev-control-053018-023834.

[13] L. A. T. Vu, Z. Bi, D. Mueller, and N. Younis, "Modular Self-Configurable Robots—The State of the Art," *Actuators*, vol. 12, no. 9, p. 361, Sep. 2023, doi: 10.3390/act12090361.

[14] B. Wang, W. Zhang, J. Luo, and Q. Xu, "Design of a Modular Wall-Climbing Robot with Multi-Plane Transition and Cleaning Capabilities," *Biomimetics*, vol. 10, no. 7, p. 450, Jul. 2025, doi: 10.3390/biomimetics10070450.

[15] Q. Zhang, X. Gao, M. Li, Y. Wei, and P. Liang, "DP-Climb: A Hybrid Adhesion Climbing Robot Design and Analysis for Internal Transition," *Machines*, vol. 10, no. 8, p. 678, Aug. 2022, doi: 10.3390/machines10080678.

[16] D. J. Miller and R. C. Lennox, "An object-oriented environment for robot system architectures," in *Proceedings., IEEE International Conference on Robotics and Automation*, IEEE Comput. Soc. Press, pp. 352–361. doi: 10.1109/ROBOT.1990.126001.

[17] C. Zieliński, "Object-oriented robot programming," *Robotica*, vol. 15, no. 1, pp. 41–48, Jan. 1997, doi: 10.1017/S0263574797000064.

[18] S. Maclean and S. Smith, "Object-oriented programming for embedded systems," *ACM SIGPLAN Notices*, vol. 30, no. 9, pp. 3–8, Sep. 1995, doi: 10.1145/214448.214449.

[19] C. Gu, "Firmware Coding in the C++ and Script Languages," in *Building Embedded Systems*, Berkeley, CA: Apress, 2016, pp. 129–147. doi: 10.1007/978-1-4842-1919-5_7.

[20] I. Graessler and J. Hentze, "The new V-Model of VDI 2206 and its validation," *at - Automatisierungstechnik*, vol. 68, no. 5, pp. 312–324, May 2020, doi: 10.1515/auto-2020-0015.